Silver-Coated Rose Petal: Green, Facile, Low-Cost and Sustainable Fabrication of a SERS Substrate with Unique Superhydrophobicity and High Efficiency

Bin-Bin Xu, Yong-Lai Zhang, Wen-Yi Zhang, Xue-Qing Liu, Jian-Nan Wang, Xu-Lin Zhang, Dan-Dan Zhang, Hao-Bo Jiang, Ran Zhang, and Hong-Bo Sun**

Recent years have witnessed a rapidly increased research interest in surface enhanced Raman scattering (SERS) spectroscopy,[1-6] because the surface-sensitive technique, so-called SERS, can directly provide the fingerprint information of various target molecules, and thus allows highly sensitive detection of analytes at very low concentration,[7] even single molecule level. To date, despite a short history, SERS has already revealed a cornucopia of both new photo-physics and practical applications in various chemical[8,9] and biological analyses.[6,10] In principle, the significantly enhanced Raman scattering of target molecules could be mainly attributed to the enhanced E-fields in the vicinity of plasmonic structures, as high as a factor of E^4.[11] Consequently, great efforts have been devoted to the fabrication of metal-based hierarchical nanostructures that can focus light into nanosized volumes[12] and form a localized surface plasmon resonance (LSPR) mode for the purpose of increasing the E-field.[13,14] To some extent, the preparation of SERS substrate shows certain dependence on the state-of-the-art of micronanofabrication techniques.[15] Despite the fact that various "top-down" and "bottom-up" approaches[16] represented by lithography,[17,18] nanoimprinting,[19] self-assembly[20] and laser direct writing[21,23] have been successfully adopted for the fabrication of periodic or rough metal nanostructures for SERS enhancement, the complexity, harsh experimental conditions and high-cost of the preparative procedures significantly limit their wide applications in various routine analysis, making the SERS detection an "in-lab-only" technique. In this regard, to achieve SERS-active substrates with nanostructure-defined LSPR in a green, facile, low cost and sustainable manner is highly desired, but obviously, it remains a scientific challenge.

On the other hand, in order to further lower the SERS detection limit, superhydrophobic surfaces have been recently adopted for the enrichment of the low-concentration analytes.[24–26] For instance, F. Gentile et al.[25] firstly reported the SERS signal of Rhodamine 6G (R6G) with an ultra-low concentration of 10^{-18} M by using superhydrophobic substrate comprising a regular lattice of silicon micro-pillar arrays covered with silver nanograin aggregates. The greatly reduced contact area between analyte solution and SERS substrate would significantly enrich the target molecules and further lower the detection limit. Besides, Z. Li et al.[26] modified silver nanoparticle coated zinc oxide nanorod arrays with stearic acid and gained one order of magnitude of detection limit less than that of hydrophilic ones, confirming the contribution of superhydrophobicity to SERS detection.

It is well known that natural creatures usually possess superhydrophobicity due to the presence of almost perfect micro-nanostructures in a wide scale range.[27,28] To date, some famous bio-prototypes such as lotus leaf,[29,30] butterfly wings,[31,32] water strider leg,[33,34] and rose petal,[35] have inspired researches to develop artificial superhydrophobic surfaces with various functionalities and broad applications. However, as far as we known, little attention has been paid to the SERS substrates derived from natural materials despite some natural nanostructures may hold great promise for achieving both LSPR and superhydrophobicity. Herein, we reported a green fabrication of highly efficient SERS-active substrate with unique surface superhydrophobicity through a facile physical vapor deposition (PVD) of silver nanolayer on natural rose petal. After silver coating, the micropapillae arrays on the petal, the sub-micron gratings on each micropapillae, and the aggregated silver nanoparticles, hereafter called nano-island, constitute the hierarchical micro-nanostructures, which contribute to not only the unique surface superhydrophobicity, but also the LSPR induced E-field enhancements. Therefore, for the first time, a novel rose-petal-based SERS substrate with high efficiency and exceptional superhydrophobicity has been successfully developed in a green, facile and sustainable fashion. As a representative illustration, R6G was used as a probing molecule for SERS experiments, and the detection limit at a level of 10^{-9} M is achieved. The biomaterial-based SERS substrates may open up a door for both facile preparation and the broad application of SERS technique in a wide range of routine analyses.

As reported elsewhere, rose petal has been proved superhydrophobic and iridescent due to the presence of periodically

---

B.-B. Xu, Dr. Y.-L. Zhang, W.-Y. Zhang, X.-Q. Liu,
J.-N. Wang, X.-L. Zhang, R. Zhang, Prof. H.-B. Sun
State Key Laboratory on Integrated Optoelectronics
College of Electronic Science and Engineering
Jilin University
2699, Qianjin Street, Changchun, 130012, PR China
E-mail: yonglaizhang@jlu.edu.cn; hbsun@jlu.edu.cn
H.-B. Jiang, Prof. H.-B. Sun
College of Physics
Jilin University
119 Jiefang Road, Changchun, 130023, PR China
D.-D. Zhang
Jiangsu Key Laboratory for Carbon-Based Functional Materials & Devices
Institute of Functional Nano & Soft Materials (FUNSOM)
Soochow University
199 Ren-Ai road, Suzhou, 215123, China

DOI: 10.1002/adom.201200019

distributed micronanostructures on the surface,[36] in this regard, we choose rose petals as superhydrophobic substrates for the fabrication of SERS detection platform. The whole experimental procedure is very simple, in our work, dried white rose petals were coated with a silver nanolayer by physical vapor deposition (PVD). Before silver coating, the dried white rose petal was characterized by SEM. As shown in **Figure 1**a, the petal takes on yellow color (inset of Figure 1a); on the surface of the petal, there exist homogeneously distributed micropapillae arrays, which are responsible for the surface superhydrophobicity. Typically, the fresh white rose petals exhibit sticky superhydrophobicity, represented by both high static water contact angle (CA) and high adhesion force, which is similar to that of *rosea Rehd*; whereas the dried petals represent a high water contact angle (CA) and a small sliding angle (SA), which is similar to that of *Rosa Hybrid Tea, cv. Showtime*. In our work, the dried petal shows a water CA as high as 158°, indicating the superhydrophobic property. Beside, the SA was measured to be ~7°, which suggests a self-cleaning property (Figure 1b). Magnified SEM image shows that, unlike the fresh rose petal, the wizened micropapillaes on the dried petal becomes scallop-like flakes due to the loss of water from cells (Figure 1c). It could be identified that the wizened micropapillaes distribute randomly on the petal; and the average size of the micropapillae is measured to be ~30 μm. SEM image of the petal profile shows that the height of the micropapillae is about 25 μm. As compared with fresh rose petal, the significantly increased spacing between neighboring micropapillaes after the loss of water may lead to a transition to the Cassie-Baxter regime and the formation of air pockets after contact with water droplets, which therefore result in high static CA and small SA. It is worth noting that there exist flexuous grooves and ordered gratings with sub-micron periods on the top and sidewall of the wizened micropapillaes, respectively (Figure 1d–f). The nanostructures may hold great promise for the surface superhydrophobicity and the formation of LSPR.

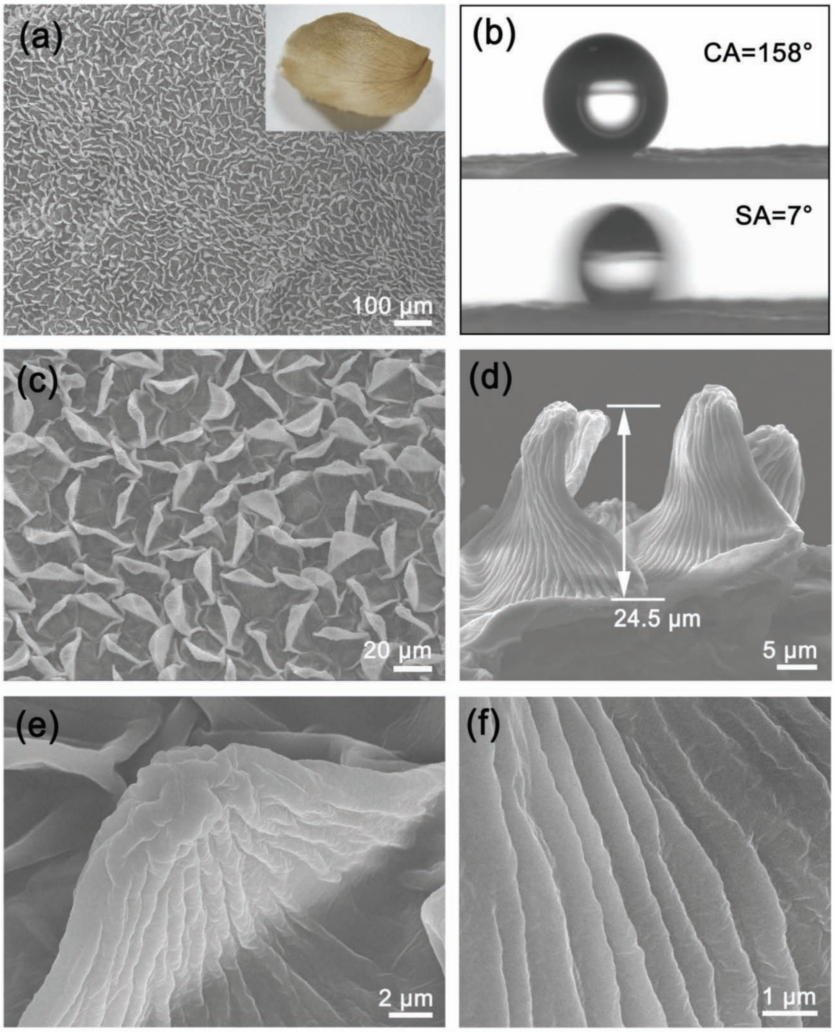

Figure 1. (a) SEM image of the dried white rose petal. The inset is the photograph of the rose petal. (b) A water droplet CA and SA of the dried rose petal. (c) Magnified SEM image of the rose petal surface. (d) Profile of the dried rose petal, the height of the micropapillaes on the petal was measure to be ~24.5 μm. (e) Magnified SEM image of a micropapillae. Naongrooves could be observed on both the top and the walls of the micropapillae. (f) SEM image of the nanograting structure on the wall of the micropapillaes.

For the preparation of SERS substrates, the dried rose petals were coated with a 30 nm of silver nanolayer as surface plasmons functional interface by physical vapor deposition (PVD). As shown in **Figure 2**a, the color of the dried rose petal changed from dark yellow to dark gray after PVD coating, indicating the presence of silver nanolayer (inset of Figure 2a). SEM images reveal that the morphology of the rose petal after silver coating do not shows any obvious changes considering the thickness of the silver nanolayer is only ~30 nm. Consequently, despite the surface chemical composition was changed due to the silver coating, the static CA and the SA were almost constant, which slightly decrease to 157° and to 10°, respectively. The magnified SEM images (Figure 2d,e) demonstrate that the silver nano-island covered the whole micropapillaes, and therefore, three-level hierarchical structures including micropapillaes, sub-micron grooves/gratings, as well as silver nano-island are formed. Notably, the gratings which were arranged almost in parallel with a width of 800 nm and depth of 500 nm extend from the bottom to the top, which are responsible for the increase of E-field intensity and the formation of "hot spots", contributing to SERS enhancement.

The silver nanolayer has been characterized by Energy-dispersive X-ray (EDX) and X-ray photoelectron spectroscopy (XPS). The EDX spectrum (supporting Figure S1) shows that three main elements (C, O, Ag) were detected, indicating the presence of silver. XPS spectrum indicates that the chemical state of the silver nanolayer is mainly Ag^0 (supporting Figure S2). Figure S3 shows the photograph of the rose-petal-based SERS substrate, the silver coated rose petals could

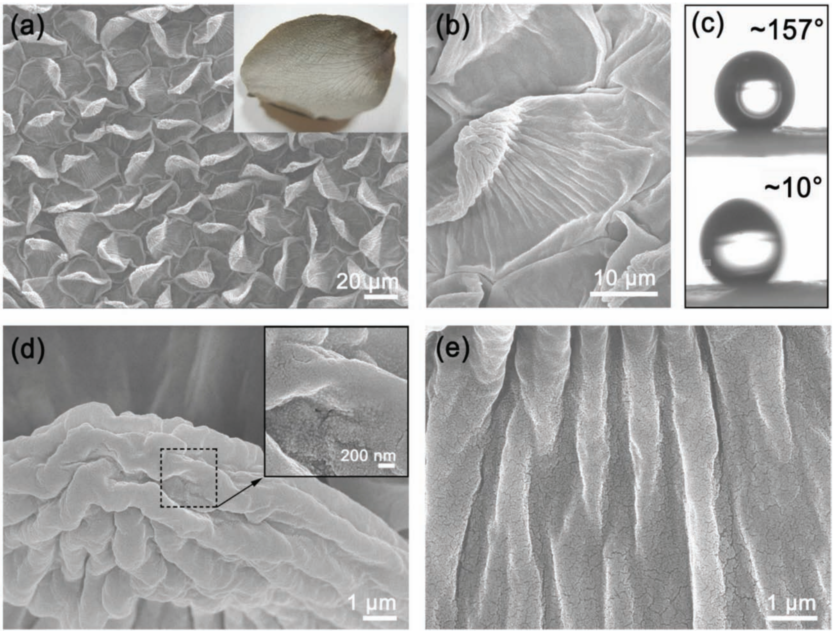

Figure 2. (a) SEM image of the silver coated rose petal. The inset is the photograph of the silver coated rose petal. (b) SEM image of a single silver coated micropapillae. (c) A water droplet CA and SA of the rose petal after silver coating. (d) Magnified SEM image of the top of a micropapillae, nanogrooves could be observed on the top. The inset is the high-resolution SEM image of the nanogrooves surface, silver nanoparticles could be identified. (e) Magnified SEM image of the nanograting on the wall of the micropapillae.

be easily tailored into various shapes and size. Additionally, for long time storage, the rose-petal-based SERS substrates could be encapsulated with polymer films to avoid oxidation.

As the silver coated rose petal exhibits hierarchical roughness, the resultant petal-based SERS substrate reveals unique surface superhydrophobicity. As shown in **Figure 3**, when a droplet of R6G aqueous solution with concentration of 10^{-6} M was dropped on the silver rose petal, the R6G droplet takes on a quasi sphere shape, indicating the superhydrophobicity. The initial volume of the R6G solution is about 7 μL, and the color is pale pink (Figure 3a). With the evaporation of water, the volume decreases obviously, and the solution color becomes deep gradually, indicating the enrichment of the R6G solution (Figure 3b). After all the solvent was evaporated, a tiny pink spot was left on the petal (Figure 3c); the final spot area, as shown in Figure 3d, is measured to be an ellipse with a major axis of 1.4 mm and a minor axis of 1.2 mm. Magnified SEM image shows that the condensed R6G molecules adsorbed on the silver petal and formed a thin film which could be easily identified form the significantly shallowed grooves on the micropapillaes.

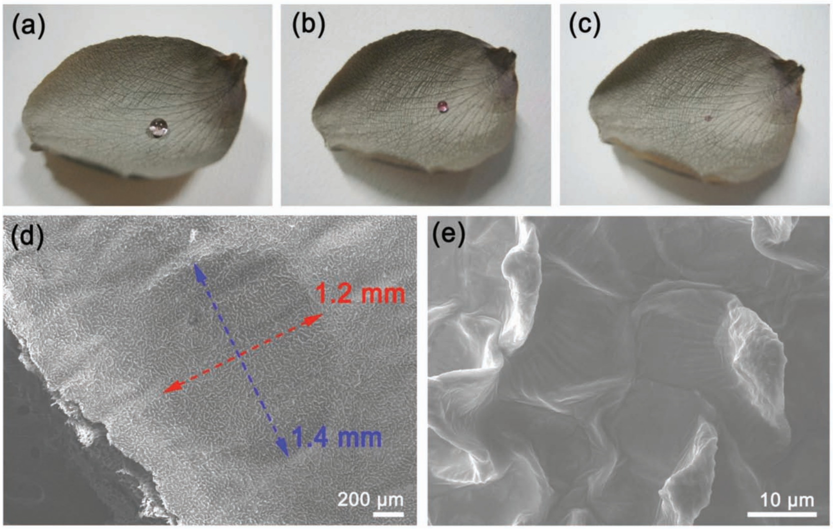

Figure 3. (a) Photograph of a droplet of R6G solution (10^{-6} M) on the silver coated rose petal. (b) With the evaporation of water, the R6G droplet became smaller and smaller, and the color darken, indicating the enrichment of the R6G droplet. (c) After drying, a R6G spot could be observed on the silver coated rose petal. (d) SEM image of the silver coated rose petal with a R6G spot. (e) Magnified SEM image of the R6G coated region.

In addition to the enrichment effect derived from the surface superhydrophobicity, the surface plasmons excited at the surface micronanostructures could also improve the SERS sensitivity through increasing the E-field intensity. Here, both the sub-micro nanogratings and the silver nano-island have been taken into account. In ordered to quantificationally investigate their contribution to E-field enhancement, the finite difference time domain (FDTD) method has been adopted for the simulation of the E-field component E_X distribution at the silver micronanostructures. **Figure 4**a shows the SEM of nanogratings on the micropapillaes, a quasi parallel nanograting structure with an average period of 800 nm and a deepness of 800 nm could be observed. FDTD simulation based on such structures shows that the maximum SERS enhancement contributed by the metal nanogratings can reach 10^5. Besides, the silver nano-island formed due to the aggregation of nanoparticles (Figure 4c) also contributes to the enhancement of SERS signal. Figure 4c shows the SEM image of local silver nanoisland, the particle size was in the range of 20 to 30 nm. Figure 4d show the E_X distribution simulation of silver nanoparticals (25 nm) located with random distance from 0, 1, 2, 5, 10 nm. The largest enhancement of E-field intensity appears mostly in slit or tip position, with a maximum enhancement of ~10^7. The FDTD simulation results reveal that the sub-micron grating structure and the silver nanoisland would contribute the major enhancement of the E-field. In addition, it is worth pointing out that the E-field enhancement shows strong dependence on the incident wavelength. For comparison, the simulation of the E-field intensity

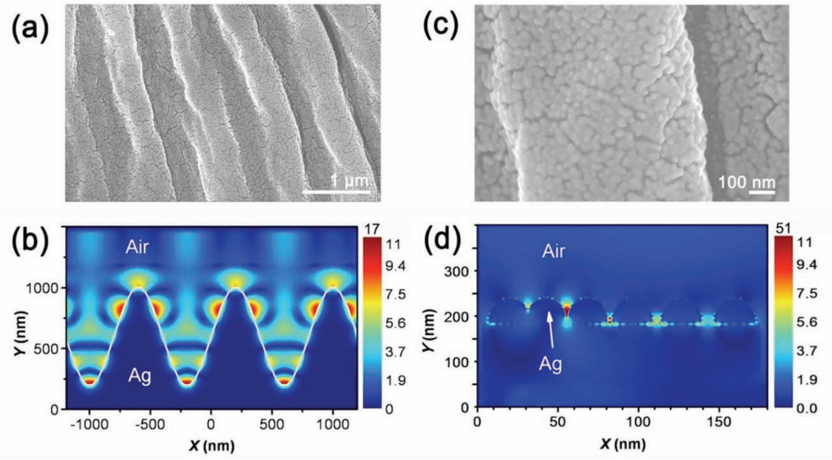

Figure 4. (a) SEM image of the typical nanograting structure on the micropapillae of the silver coated rose petal. (b) FDTD stimulation of the E-field intensity distribution with incident laser wavelength of 514 nm at the nanograting structure (period 1.6 µm, depth 800 nm, sinusoid). (c) High-resolution SEM image of silver nano-island. (d) E_X distribution simulation with incident laser wavelength of 514 nm of silver nanoparticals (hemisphere, 25 nm in diameter) located with a distance of 0, 1, 2, 5 and 10 nm (from left). For color version, please see the supporting information.

distribution with incident laser wavelength of 633 and 800 nm has also been carried out. As shown in Figure S4 and S5 (supporting information), the E_X distribution varied obviously with different incident wavelength.

To investigate the detection capabilities of our rose-petal-based SERS substrate, we choose R6G as probe molecule. In our experiment, a droplet of R6G aqueous solution with a concentration of 10^{-9} M was dropped on the silver rose petal, followed by the evaporation of water solvent. We randomly selected 15 different probe sites, including 7 sites on the top grooves and 8 sites on the bottom gratings. The SERS spectra of R6G are shown in **Figure 5**a, some characteristic bands of R6G (at 611, 1360, 1507 and 1651 cm^{-1}) were detected in a strong intensity, indicating the exceptional SERS enhancement. The reproducibility of our SERS substrates have also been evaluated, as shown in Figure 5b, the peak intensity of the band at 1651 cm^{-1} was chosen as a parameter to evaluate the reproducibility of its SERS enhancement. The consistency of SERS signals confirms the homogeneous property of the rose petal based SERS substrate. The SERS enhancement factor was calculated to be ~10^8 (for the detail of the calculation, see the supporting information and Figure S7). In fact, at the concentration of 10^{-10}, SERS signal could also be collected at a signal-to-noise ratio of ~3 (Figure S8). In our experiments, only the spectrum with signal-to-noise lager than 3 could be considered as effective signal, so the detection limit of our rose-petal-based SERS substrates was estimated to be 10^{-9} mol/L.

In conclusion, we have developed a highly efficient SERS substrate through a facile PVD coating of silver nanolayer on natural rose petal. The presence on hierarchical micronanostructures including micropapillae arrays, submicron grooves and grating, as well as silver nano-island contribute to not only surface superhydrophobicity, but also significantly enhanced local E-field intensity. The former shows exceptional enrichment effect for low concentration analytes, and thus lower the SERS detection limit; whereas the later gives rise to the formation of SERS "hot spots" due to the LSPR. By using the rose-petal-based SERS substrate, the SERS detection limit as low as 10^{-9} M has been achieved, and the SERS enhancement factor of the silver rose petal is estimated to be 10^8. The use of natural flower petals for SERS substrates is not limited to rose, other petals with suitable micronanostructures could also be adopted to further optimize the SERS enhancements, and lower the detection limit. Moreover, by selecting the suitable surface structures of other petals that could match the incident wavelength, and carefully modulating the silver thickness, the performance of the SERS substrate is expected to be further improved. The green, facile, low-cost and sustainable preparation of highly efficient SERS substrates based on rose petal show enormous value on both scientific research and commercial prospect.

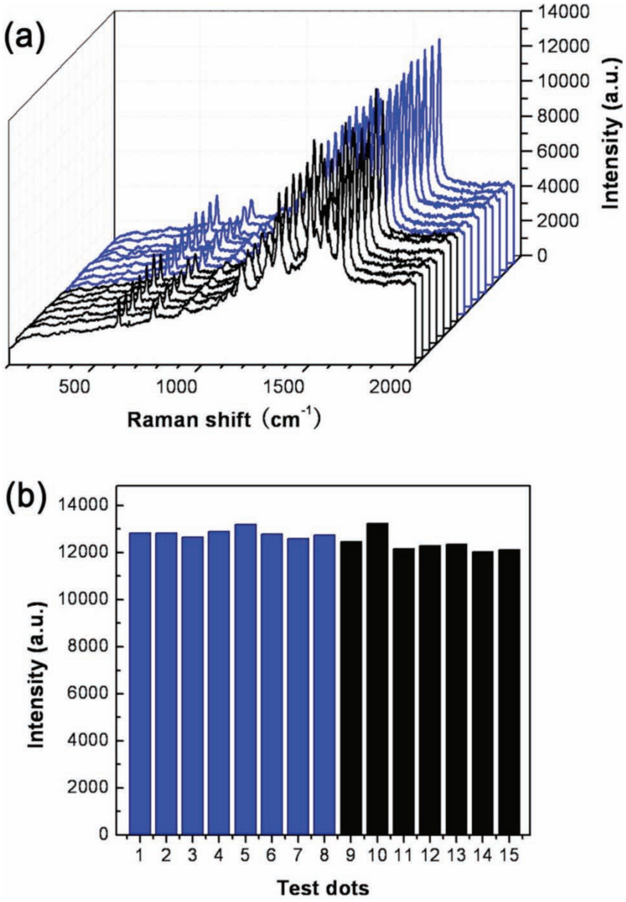

Figure 5. Raman spectra of a R6G droplet (10^{-9} M) on the silver coated rose petal. The blue spectra are SERS signals collected on the top of the micropapillae, whereas the black spectra are collected on the nanograting structures. (b) The peak intensity of the 15 measured sites at the band of 1651 cm^{-1}.

Experimental Section

Sample Fabrication and Characterization: The fresh white rose petals were dried in ambient environment. The corresponding silver rose petals served as the SERS-active enabler were fabricated by physical vapor deposition (PVD) coating of a silver layer on dried white rose petals. Deposition rate of silver was about 0.15 nm/s. JEOL JSM-6700F field emission scanning electron microscope (FE-SEM) was used to measure the surface morphologies of the samples. EDS, XPS CAs and SAs were measured using an OCA20 system (Dataphysics GmbH, Germany). Raman spectra were recorded on a JOBIN YVON T64000 equipped with a liquid-nitrogen-cooled argon ion laser at 514.5 nm (Spectra-Physics Stabilite 2017) as excitation source, the laser power used was about 10 mW at the samples with an average spot size of 1 μm in diameter.

Physical Vapor Deposition (PVD) Coating Silver Film: We coated the rose petals with silver film prepared by thermal evaporation using thermal evaporation system DM-300B. The PVD process was finished in a high vacuum (less than 5×10^{-4} Pa), the silver powder was placed in molybdenum boat and applied an electric current of 70 A.

Simulation: E-field component E_X distribution simulation of the silver nanogratings region was implemented by the finite difference time domain (FDTD). The period of simulated silver nanogratings is about 800 nm and the deepness is about 500 nm. The E_X distribution was simulated by using silver nanoparticals (hemishere, 25 nm in diameter) as models, which located with random distance of 0, 1, 2, 5 and 10 nm.

Supporting Information

Supporting Information is available from the Wiley Online Library or from the author.

Acknowledgements

The authors gratefully acknowledge support from NSFC (Grant Nos. 90923037, 61008014 and 60978048). We also acknowledge the China Postdoctoral Science Foundation No. 20110490156 and the Hong Kong Scholar Program XJ2011014. This work is also supported by PhD interdisciplinary project Nos. 450091102507 and 450060483105, Jilin University.

Received: October 22, 2012

[1] D. Choi, Y. Choi, S. Hong, T. Kang, L. P. Lee, *Small* **2010**, *6*, 1741.

[2] Y. Yokota, K. Ueno, H. Misawa, *Chem. Commun.* **2011**, *47*, 3505.

[3] X. X. Han, L. J. Cai, J. Guo, C. X. Wang, W. D. Ruan, W. Y. Han, W. Q. Xu, B. Zhao, Y. Ozaki, *Anal. Chem.* **2008**, *80*, 3020.

[4] X. Jiang, X. Li, X. Jia, G. Li, X. Wang, G. Wang, Z. Li, L. Yang, B. Zhao, *J. Phys. Chem. C* **2012**, *116*, 14650.

[5] Y. Zhao, X.-J. Zhang, J. Ye, L.-M. Chen, S.-P. Lau, W.-J. Zhang, S.-T. Lee, *ACS Nano* **2011**, *5*, 3027.

[6] Y. He, S. Su, T. Xu, Y. Zhong, J. A. Zapien, J. Li, C. Fan, S.-T. Lee, *Nano Today* **2011**, *6*, 122.

[7] M.-W. Shao, L. Lu, H. Wang, S. Wang, M.-L. Zhang, D.-D.-D. Ma, S.-T. Lee, *Chem. Commun.* **2008**, 2310.

[8] B.-B. Xu, R. Zhang, X.-Q. Liu, H. Wang, Y.-L. Zhang, H.-B. Jiang, L. Wang, Z.-C. Ma, J.-F. Ku, F.-S. Xiao, H.-B. Sun, *Chem. Commun.* **2012**, *48*, 1680.

[9] W. Ji, X. Xue, W. Ruan, C. Wang, N. Ji, L. Chen, Z. Li, W. Song, B. Zhao, J. R. Lombardi, *Chem. Commun.* **2011**, *47*, 2426.

[10] J. Ando, K. Fujita, N. I. Smith, S. Kawata, *Nano Lett.* **2011**, *11*, 5344.

[11] E. C. Le Ru, P. G. Etchegoin, *Chem. Phys. Lett.* **2006**, *423*, 63.

[12] Y.-H. Chen, L. Huang, L. Gan, Z.-Y. Li, *Light Sci. Appl.*, **2012**, *1*, e26.

[13] L. Wang, W. Xiong, Y. Nishijima, Y. Yokota, K. Ueno, H. Misawa, J. Qiu, G. Bi, *Appl. Opt.* **2011**, *50*, 5600.

[14] Y. Jiang, H.-Y. Wang, H. Wang, B.-R. Gao, Y.-w. Hao, Y. Jin, Q.-D. Chen, H.-B. Sun, *J. Phys. Chem. C* **2011**, *115*, 12636.

[15] C. Tian, C. Ding, S. Liu, S. Yang, X. Song, B. Ding, Z. Li, J. Fang, *ACS Nano* **2011**, *5*, 9442.

[16] J. Wang, Y. Zhang, S. Wang, Y. Song, L. Jiang, *Acc. Chem. Res.* **2011**, *44*, 405.

[17] C. Edwards, A. Arbabi, G. Popescu, L. L. Goddard, *Light Sci. Appl.* **2012**, *1*, e44.

[18] B.-B. Xu, Z.-C. Ma, H. Wang, X.-Q. Liu, Y.-L. Zhang, X.-L. Zhang, R. Zhang, H.-B. Jiang, H.-B. Sun, *Electrophoresis* **2011**, *32*, 3378.

[19] B. D. Lucas, J.-S. Kim, C. Chin, L. J. Guo, *Adv. Mater.* **2008**, *20*, 1129.

[20] Y.-H. Su, Y.-F. Ke, S.-L. Cai, Q.-Y. Yao, *Light Sci. Appl.* **2012**, *1*, e14.

[21] B.-B. Xu, Z.-C. Ma, L. Wang, R. Zhang, L.-G. Niu, Z. Yang, Y.-L. Zhang, W.-H. Zheng, B. Zhao, Y. Xu, Q.-D. Chen, H. Xia, H.-B. Sun, *Lab Chip* **2011**, *11*, 3347.

[22] Y.-L. Zhang, Q.-D. Chen, H. Xia, H.-B. Sun, *Nano Today* **2010**, *5*, 435.

[23] W. Xiong, Y. S. Zhou, X. N. He, Y. Gao, M. Mahjouri-Samani, L. Jiang, T. Baldacchini, Y. F. Lu, *Light Sci. Appl.* **2012**, *1*, e6.

[24] R. Zhang, B.-B. Xu, X.-Q. Liu, Y.-L. Zhang, Y. Xu, Q.-D. Chen, H.-B. Sun, *Chem. Commun.* **2012**, *48*, 5913.

[25] F. Gentile, G. Das, M. L. Coluccio, F. Mecarini, A. Accardo, L. Tirinato, R. Tallerico, G. Cojoc, C. Liberale, P. Candeloro, P. Decuzzi, F. De Angelis, E. Di Fabrizio, *Microelectron. Eng.* **2010**, *87*, 798.

[26] F. Xu, Y. Zhang, Y. Sun, Y. Shi, Z. Wen, Z. Li, *J. Phys. Chem. C* **2011**, *115*, 9977.

[27] D. Liu, Z. Wang, X. Jiang, *Nanoscale* **2011**, *3*, 1421.

[28] K. Liu, X. Yao, L. Jiang, *Chem. Soc. Rev.* **2010**, *39*, 3240.

[29] L. Feng, S. Li, Y. Li, H. Li, L. Zhang, J. Zhai, Y. Song, B. Liu, L. Jiang, D. Zhu, *Adv. Mater.* **2002**, *14*, 1857.

[30] D. Wu, J.-N. Wang, S.-Z. Wu, Q.-D. Chen, S. Zhao, H. Zhang, H.-B. Sun, L. Jiang, *Adv. Funct. Mater.* **2011**, *21*, 2927.

[31] K. Chung, S. Yu, C.-J. Heo, J. W. Shim, S.-M. Yang, M. G. Han, H.-S. Lee, Y. Jin, S. Y. Lee, N. Park, J. H. Shin, *Adv. Mater.* **2012**, *24*, 2375.

[32] P. Vukusic, J. R. Sambles, *Nature* **2003**, *424*, 852.

[33] X. J. Feng, L. Jiang, *Adv. Mater.* **2006**, *18*, 3063.

[34] X. Gao, B. B. Snider, *ChemInform* **2004**, *35*, no.

[35] B. Bhushan, E. K. Her, *Langmuir* **2010**, *26*, 8207.

[36] L. Feng, Y. Zhang, J. Xi, Y. Zhu, N. Wang, F. Xia, L. Jiang, *Langmuir* **2008**, *24*, 4114.